ACS APPLIED MATERIALS & INTERFACES

www.acsami.org Research Article

Robust Microcapsules with Durable Superhydrophobicity and Superoleophilicity for Efficient Oil–Water Separation

Wenjun Luo, Dawei Sun, Shusheng Chen, Logesh Shanmugam, Yong Xiang,* and Jinglei Yang*

Cite This: *ACS Appl. Mater. Interfaces* 2020, 12, 57547–57559 Read Online

ACCESS | Metrics & More | Article Recommendations | Supporting Information

ABSTRACT: The poor ultraviolet (UV) resistance and insufficient solvent compatibility are challenges for long-term storage and service of oil–water separation materials in practical applications. Herein, a superhydrophobic/superoleophilic surface with nano- to microscale hierarchical structures was formed spontaneously on robust microcapsules (MCs) via in situ polymerization and a sol–gel surface treatment. The resultant MCs possessed superior UV-resistant and solvent-proof superhydrophobicity. The water contact angles (WCAs) of the MC coating remained above 160° and the sliding angles (SAs) were below 3° after 9 days of UV aging test or 20 days of nonpolar and polar aprotic solvent immersion tests. More interestingly, these MCs can be used to separate the oil phase from its aqueous emulsion effectively, achieving a high and reusable separation efficiency with over 90% oil purity after 10 cycles of filtrations even after 13 days of UV aging. Therefore, these novel MCs will exhibit effective oil–water separation performance, superior chemical stability, outstanding reusability, and long-term storage stability for promising practical applications.

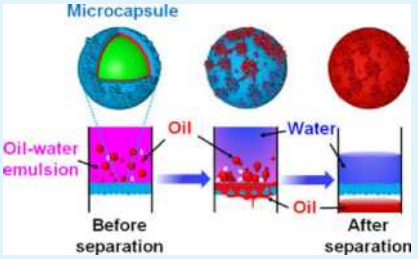

KEYWORDS: *microcapsules, superhydrophobicity, superoleophilicity, sol–gel surface treatment, durability, long-term storage stability, oil–water separation*

1. INTRODUCTION

The rapid development of human society has increased the frequency of accidents involving oil spills and oil effluent discharge, which have seriously threatened the aquatic ecological environment.[1−3] Oil–water separation materials have attracted great interest in recent years for different applications, ranging from oil spill treatment, water remediation, to oil moisture removal.[4−6] The conventional materials used to separate and remove oils and organic stains from water by chemical etching,[7] CVD techniques,[8] hydrothermal methods,[9] layer-by-layer processes,[10] and others[11,12] include sorbents and membranes. An ideal absorbent material possesses high absorption potential and excellent recyclability. Most of the oil sorbents used to remove oily substances from water are based on porous structures, including aerogels,[13,14] CNF functional aerogels,[15] hierarchical-structured aerogels,[16] GP frameworks,[17,18] carbon nanotube sponges,[19] and foams with magnets.[20] The kinds of membranes developed for effective oil–water separation, in addition to oil sorbents, include ceramic hollow fiber microfiltration membranes,[21] photosensitive sol–gel-modified membranes,[22] ZrO_2-modified alumina membranes,[23] polyethylene glycol surfactant-modified glass membranes,[11] and zeolite microfiltration membranes.[24] However, these membranes were only sufficient for prefiltering of oil substances from the oil–water mixture, and it was a critical matter that membranes were prone to contamination and were hard to clean, which significantly hampered their practical application. Most of the oil sorbents not only have weakened UV resistance (e.g., TiO_2-modified ceramic membranes[25]), which will be indispensable to induced material photodegradation, but also have a complicated preparation process, poor recyclability, high costs, the low oil sorption capacity and the challenges of scalability inherent in these methods significantly restrict their practicality.[26] Therefore, it was important to develop a highly effective separation material that can be easily manufactured on a scale up for the sustainable production of materials for dealing with oil-polluted water and oil spills.

Superhydrophobic surfaces, described as those with a water contact angle above 150 ° and a sliding angle (SA) below 10 °, are of specific interest in both science and industrial communities for their wetting properties.[27−29] Most researchers attributed the superhydrophobicity to an amalgamation of surface roughness on nano/microscales and surface chemical properties. In addition, low surface tension liquids such as different oils would spread rapidly over the superhydrophobic surface since the surface energy with high roughness was close to that of oils, and the superhydrophobic surface generally showed superoleophilicity. The wettability of solid surfaces

Received: August 27, 2020
Accepted: November 20, 2020
Published: December 10, 2020

https://dx.doi.org/10.1021/acsami.0c15455
ACS Appl. Mater. Interfaces 2020, 12, 57547−57559

could be adjusted via modifying the geometric surface structure and the surface chemical properties of the material.[30] Recently, for the increased separation of oils or organic contaminants from water, sorbents and membranes with not only superhydrophobicity but also superoleophilicity have been broadly created. For example, Zhu et al.[31] reported superhydrophobic and superoleophilic sponges, which were fabricated based on $AgNO_3$/n-dodecanoic acid, but the absorption ability of these sponges was 13 times their weight. Zhang et al.[32] reported that through the process of a physical−chemical foaming system, plasma surface treatment, and silane modification, superhydrophobic aerogels based on cellulose were fabricated, which had a high oil sorption ability of up to 43 times their weight. Ke et al.[33] reported a versatile process method based on polymerized octadecylsiloxane (PODS) coatings for superhydrophobic sponges that firmly bind to the sponge, resulting in 42−68 times the absorption ability of the PODS-sponge weight for oil after 50 cycles of separation. Moreover, using a drop-coating method, a novel sponge was prepared to deposit fluoroalkyl silane-modified Fe_3O_4 NPs onto a magnetic melamine (MA) sponge; Li et al.[34] reported that the surface-modified MA sponge could isolate organic solvents from water and efficiently absorb various oils, with a maximum absorption capacity ranging from 59 to 77 g/g. In addition, various superhydrophobic membranes, including polyimide nanofibrous membranes,[35] PVDF-based membranes,[36] and CNT films,[37] have also been fabricated. In addition to the ability to separate oil and water, Yu et al.[38] reported that a chemically stable fabric called dye-sensitized TiO_2-TEOS/VTEO was developed for further purification of water-soluble pollutants with no fluorine, and this modified polyester showed WCAs >125° after 22 abrasion cycles, poor chemical properties, and above 95% oil−water mixture separation efficiency (WCAs >145°) after 24 separation cycles. Su et al.[39] reported that through a simple approach using a cheap sol−gel process, a superhydrophobic polyester textile was fabricated, and this modified textile showed outstanding chemical resistance properties and mechanical robustness and exhibited above 90% excellent efficiency (WCAs >150°) and reusability after 30 separation cycles in an oil−water mixture. In particular, another point about UV resistance performance was seldom discussed; Xue et al.[40] synthesized a superhydrophobic textile for oil−water mixture separation with durability against laundering and abrasion and excellent solvent robustness on long-time exposure to 140 h UVA (WCAs > 160°); this modified fabric was synthesized via the development of rough structures through the process of fiber alkali etching, mercapto silane modification, and hydrophobization by thiol-ene click chemistry.

Nevertheless, most of these superhydrophobic sorbents or membranes were modified via the introduction of an extremely wettable surface on the existing substrates, and the generated surface layer had poor degradability, especially when they were exposed to an environment of high ultraviolet intensity and chemical substances.[41,42] In addition, a downside is that most of the materials could not separate oil substances from surfactant-stabilized oil−water emulsions.[43] Therefore, the development of an effective fabrication method for oil−water separation materials was more desirable with high separation efficiency, superior chemical stability, outstanding reusability, and long-term storage stability.

Herein, we demonstrated a simple fabrication of microcapsules with durable superhydrophobic and superoleophilic features for the efficient separation of oil droplets from a mixture or emulsion. These microcapsules were modified by a sol−gel surface treatment between (3-aminopropyl) triethoxysilane (APTES) and tetraethyl orthosilicate (TEOS). The superhydrophobicity was due to the diffusion of low surface energy core material and subsequent spontaneous chemical modification on the surface of the resulting microcapsules. The newly developed microcapsules exhibited a distinct chemical composition with superior UV resistance and excellent solvent-proof superhydrophobicity. More interestingly, these robust microcapsules had demonstrated a remarkable capacity to extract small oil droplets from emulsions with a high separation efficiency after multiple cycles of filtration and long-lasting UV aging. Our findings confirmed the ability of the new method to synthesize a robust microcapsule with effective oil−water separation performance, superior reusability, and long-term storage stability for real-world applications in oil spill accidents and industrial wastewater treatments.

2. EXPERIMENTAL DETAILS

2.1. Materials. 1-Hexadecanol (cetyl alcohol) was purchased from Alfa Aesar, Thermo Fisher Scientific Co., Ltd. Butyl acetate (BuA) and aqueous ammonia ($NH_3{\cdot}H_2O$, 25.0%, w/v) were provided by Wako Pure Chemical Industries, Ltd. (Japan); deionized water with a resistivity higher than 18.2 MΩ·cm was used in all formulations. The following chemicals were purchased from Sigma-Aldrich: dibutyltin dilaurate, TEOS, APTES, isophorone diisocyanate (IPDI), resorcinol, aqueous solution of formaldehyde (37.0%, w/v), citric acid, ethylene maleic anhydride (EMA), triethanolamine, methanol, bromophenol blue, Sudan III, di-n-butylamine solution, anhydrous *n*-hexane, and anhydrous chloroform. Anhydrous toluene, acetone, and isopropyl alcohol were purchased from Duksan Pure Chemicals Co., Ltd. Anhydrous acetone, acetonitrile, dimethylformamide (DMF), dichloromethane (DCM), diethyl ether, and xylene were obtained from VWR Chemicals Limited. Unless otherwise mentioned, all the chemicals in this analysis were used without further purification.

2.2. Preparation of Microcapsules (MCs). *2.2.1. Synthesis of Hydrophobic Core Material (C_{16}-IPDI).* Appropriate amounts of BuA and IPDI were stirred and put into a three-neck round-bottom flask under temperature control. The solution was filled with N_2. The flask was then heated to 50 °C. After this, a blend of 1-hexadecanol and BuA was added dropwise into the glass flask with continuous mechanical stirring. The hydroxyl (from 1-hexadecanol)/isocyanate (from IPDI) molar ratio was maintained at 1:1. 0.1% Dibutyltin dilaurate of the total weight (alcohol and IPDI) acting as a catalyst was added, and this reaction was continued for another hour. Finally, a clear solution containing the hydrophobic core material (e.g., C_{16}-IPDI) was obtained.

2.2.2. Synthesis of Poly(Urea−Formaldehyde) (PUF) MCs Containing C_{16}-IPDI. In the initial stage of this process, PUF MCs containing C_{16}-IPDI were prepared via the in situ polycondensation process based on Brown et al.'s study.[44] The experimental procedure for fabricating C_{16}-IPDI MCs was as follows: a triethanolamine aqueous solution was used for regulating the pH value of the formaldehyde aqueous solution (6.5 g, 37 wt %) to about ∼8. Then, 2.5 g of urea was added to this alkaline aqueous solution in a 20 mL glass vessel. This vessel was kept in a water bath and placed on a hotplate at a preset temperature of 75 °C under mechanical stirring. After reacting for 60 min, the prepolymer of the urea−formaldehyde (PUF) aqueous solution was obtained. Next, 40 g of ultrapure water and 17 g of 3.0 wt % EMA aqueous solution was poured into a 500 mL beaker. The prepared PUF solution was then added, and the blend was agitated through a propeller at an agitation rate (200 rpm) at 24 °C for 10 min. Subsequently, 8 g of the oil phase (C_{16}-IPDI) was added into the water solution at 22 °C under an increased agitation rate of 800 rpm for 20 min to proceed the emulsification process. After the emulsion system was stabilized for 20 min, the pH value of the system was then regulated to about 1.3 through 50.0 wt %

https://dx.doi.org/10.1021/acsami.0c15455
ACS Appl. Mater. Interfaces 2020, 12, 57547−57559

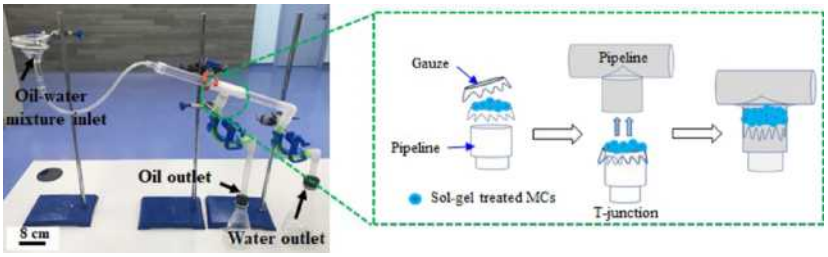

Figure 1. Separation apparatus for surfactant-free oil–water mixtures and schematic diagrams of sol–gel-treated MCs mainly positioned at the T-junction pipeline.

citric acid aqueous solution (pH ~ 0.2) to initiate and facilitate in situ polymerization. To enhance the consolidation of shell generation, 0.25 g of resorcinol was then added into the reaction system. The agitation rate was decreased to 400 rpm to control the stability of C_{16}-IPDI MCs, and the reaction blend was further stirred at 22 °C for 20 min. After that, this system had been transferred into the water bath again to undergo further reaction at 55 °C under an agitation rate of 100 rpm for about 1 h. Finally, the reaction was terminated by air drying to room temperature. The obtained C_{16}-IPDI MCs were washed at least five times with deionized water and then filtered before further surface treatment.

2.2.3. Preparation of Sol–Gel-Treated MCs. A mixture of TEOS and APTES at a consistent molar ratio of 1:1 was prepared to form a homogeneous solution under room temperature, and 10 g of C_{16}-IPDI MCs was added to this mixture. After continuous mechanical stirring for a few minutes, the surface treatment was first allowed to atomize with a vapor of alkali solution (methanol:$NH_3{\cdot}H_2O$:H_2O = 3:1:1, v/v/v) for 20 min in a sealed chamber. Consequently, the pretreated C_{16}-IPDI MCs were equilibrated at a certain temperature (e.g., 70 °C), and the reaction time for the sol–gel vapor surface treatment was increased to 60 min in the presence of dibutyltin dilaurate. The sol–gel-treated MCs were finally obtained after being air-dried overnight in a fume hood.

2.3. Characterization of Microcapsules. The status of the MCs during the synthetic process was monitored using a Leica DM2700 M optical microscope (OM) equipped with a bright LED illumination lamp and a digital camera. The morphologies of the MC surfaces were investigated using a field-emission scanning electron microscope (SEM, JCM-6000PLUS NeoScope, JEOL, USA). Particle size distribution was measured using a particle size analyzer (LS13 320 MW, Beckman Coulter).

Fourier transform infrared (FTIR) spectra of the synthesis component of MCs were measured using an attenuated total reflection (ATR) accessory coupled to a Nicolet iS50 FTIR spectrometer. The chemical components on the surface of the sol–gel-treated MCs were characterized by X-ray photoelectron spectroscopy (XPS).

The surface morphologies of MCs were investigated using a Multimode 8 atomic force microscope (AFM, Bruker, USA) in the tapping mode under a scan rate of 256 Hz and a scan area of 5 μm × 5 μm at an ambient temperature. The average and standard deviation of surface roughness were checked from five different measurements recorded by optical profilometry (Bruker NPFLEX) under a scan area of 480 μm × 640 μm at different locations.

An optical contact angle meter device was used to calculate the static contact angle and the sliding angle of the water (Biolin Theta Contact Angle Meter). By tilting the stage, the SAs were calculated before the droplet rolled off the coating surface of the MCs; the volume of droplets used was 5 μL for the static contact angle and the sliding angle tests. Three measurements were carried out on each MC coating surface.

2.4. UV Aging Test of Microcapsules. The UV aging test was assessed using a QUV accelerated weathering tester (Model: QUV/Spray, Q-Lab, USA) with a UVA-340 lamp in a critical wavelength range from 365 nm down to the shortcut of 295 nm. The UVA photodegradation investigation was halted after 8 h with irradiance (0.89 W/m^2) and halted after 4 h of condensation at a temperature of 50 °C according to ASTM G154 Cycle 1 (12 h = 1 cycle). The contact angle measurements were conducted every two cycles.

2.5. Solvent Resistance Characterizations of Microcapsules.
2.5.1. Release of Core Material in Solvents Quantified by Titration. Nonpolar solvents such as *n*-hexane, diethyl ether, xylene, and chloroform; polar aprotic solvents such as DMF, acetonitrile, acetone, and DCM; and polar protic water were taken into account in this research work. To prevent the effect of residual moisture on the measurements, all organic solvents considered were anhydrous. All processes were conducted in an oven to mitigate the impact of moisture in the atmosphere. The release rate of core materials was characterized using the following procedure:[45] the release rate (weight percent of the released substance) of the sol–gel-treated MCs was measured using 2 wt % of MCs dispersed in 10 g of extraction solvents with slight stirring (200 rpm) and then sealed in a 20 mL glass vial under room temperature. Within a certain timeframe, 2 g of the organic solvent was easily absorbed into the conical flask with a plastic dropper. The released core material in the testing solvent would be titrated based on the ASTM Standard D2572–97. In order to collect the average release percentage of the core material and its standard deviation, each specimen was titrated three times. Finally, the relative release percentage of the core material could be calculated using the equations as follows:

$$\mathrm{NCO\%} = \frac{(V_{\mathrm{blank}} - V) \times C_{\mathrm{HCl}} \times 0.042}{M_{(\mathrm{specimen})}} \times 100\% \quad (1)$$

$$M(\mathrm{released\ core}) = 2 \times M(\mathrm{solvent}) \times \frac{\mathrm{NCO\%}}{1 - 2\mathrm{NCO\%}} \quad (2)$$

$$\mathrm{Core\ release\ wt\ \%} = \frac{M_{(\mathrm{released\ core})}}{M_{(\mathrm{encapsulated\ core})}} \times 100\% \quad (3)$$

where NCO% is the percentage of the core release (NCO) from MCs in testing solvents. V_{blank} (ml) and V (ml) are the volume amounts of the regular HCl (0.1 M) solution absorbed by the trial and titration specimens, respectively. C_{HCl} is the aqueous solution of HCl (0.1 M), 0.042 is the mass of the NCO group, and $M_{(\mathrm{specimen})}$ (g), $M_{(\mathrm{released\ core})}$ (g), $M_{(\mathrm{solvent})}$ (g), and $M_{(\mathrm{encapsulated\ core})}$ (g) are the weights of the specimen, core material in the solvent system, solvent, and encapsulated core materials in the primary MCs, respectively.

2.5.2. Solvent Resistance of Microcapsules Via Direct Immersion. In addition, the as-fabricated MCs were also subjected to the solvent immersion test and immersed in both nonpolar solvents and polar aprotic solvents for 20 days, and subsequently, the wetting properties were investigated by contact angle measurements.

2.6. Oil–Water Separation Tests of Microcapsules.
2.6.1. Oil–Water Separation Test of Surfactant-Free Mixtures. The main accessory of the oil–water separation apparatus was designed to separate a large amount of oil–water mixture (Figure 1). Two types of selected oils (color-dyed with Sudan III), including hexane and DCM, were chosen as representatives of various densities, respectively. The oil–water mixture was composed of 400 mL of oil and 400 mL of DI water without any surfactants. As the oil spread through the T-junction, it permeated suddenly and fell continuously into an oil storage vessel. On the other side, as the water flowed

https://dx.doi.org/10.1021/acsami.0c15455
ACS Appl. Mater. Interfaces 2020, 12, 57547–57559

through the T-junction, it moved quickly and was stored in the water collection vessel.

2.6.2. Oil–Water Separation Test of Surfactant-Stabilized Emulsions. The separation device for oil–water surfactant-stabilized emulsions was operated by a vacuum-driven filtration device at a vacuum degree of −0.1 MPa (Figure 2). For surfactant-stabilized

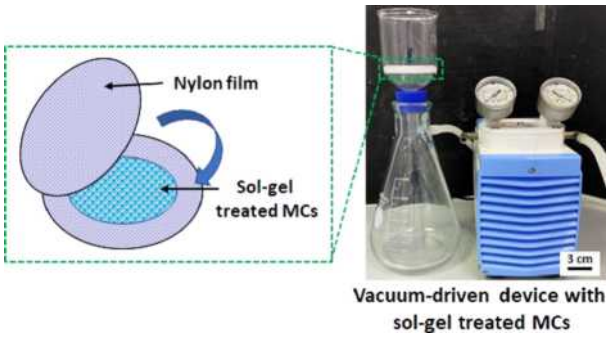

Figure 2. Schematic of the separation mechanism for surfactant-stabilized oil–water emulsion using a vacuum-driven filtration device.

hexane–water emulsion, 2.0 g of Tween 80 was mixed with 400 mL of hexane followed by addition of 400 mL of water (color-dyed with methylene blue) and the oil–water mixture was stirred for 20 min. The surfactant-stabilized DCM–water emulsion was also prepared in the same manner. All the oil–water emulsions stabilized by surfactants were stabilized for more than 1 day, and no precipitation appeared. The oil immediately infiltrated through the sandwiched construction when the emulsions were infused onto the nylon–(sol–gel-treated MC)–nylon sandwiched system from the upper glass tube of the filter system. At the same time, upon contacting the MCs, the emulsion droplets demulsified, with water maintaining in the upper glass vessel. It is possible to successfully separate all emulsions in one phase by applying a single vacuum pressure.

To verify the reusability of the oil–water separation performance of sol–gel-treated MCs, the separation process was repeated after every UV test cycle (12 h). The efficiency of oil–water mixture separation was determined by the ratio between the mass of oil collected in a vessel and calculated via the following formula

$$Q = M_0/M_1 \times 100\% \quad (4)$$

where Q is the oil separation efficiency, M_0 is the collected oil mass (g), and M_1 is the original mass of the oil added in the mixture (g).

Mixture or emulsion fluxes were calculated by measuring the amount of permeate per unit time based on the following equation (eq 5)

$$\text{Flux} = V/\text{At} \quad (5)$$

where A (m^2) is the valid filtration surface of the T-junction (1 cm in diameter) or sandwiched construction (7 cm in diameter), V (L) is the volume of the permeate, and t (h) is the separation time. A certain amount of mixture or emulsion was poured into the filter for each examination. For each device, three samples were checked to obtain an average value.

3. RESULTS AND DISCUSSION

3.1. Synthesis of Hydrophobic Core Material (C_{16}-IPDI). The C_{16}-IPDI core material could diffuse spontaneously from the MCs mainly due to the fact that isocyanates were reactive with the sol–gel-treated MCs' shell containing hydroxyl/amino groups. The hydrophobic core material was fabricated by a chemical reaction between the IPDI isocyanate groups and standard alcohol hydroxyl (Scheme 1b). After the aging time increased, the released-out isocyanates could undergo a reaction with hydroxyl/amino groups, which produced new polyurethane aggregates that distributed on the surface of the SiO_2/PUF MCs' shell (Scheme 1d).

The core material (C_{16}-IPDI) was synthesized using IPDI and 1-hexadecanol (Scheme 1b). The FTIR spectra of the core material with different reaction times are shown in Figure 3. For the specimen with 1 h of reaction time, the peak at 3335 cm^{-1} was assigned to the stretching vibration of N–H, and the peak at 2260 cm^{-1} corresponds to the stretching vibration of –NCO functional groups. The C═O group stretching at 1711 cm^{-1} was observed for the core material. The peaks at 1385 and 1090 cm^{-1} were assigned to the vibrations of $-CH_2$. A new band of the –NH peak in the FTIR spectra resulting from the urethane bond appeared at 1527 cm^{-1} during this reaction, the strength of which gradually increased in 4 h and then leveled-off. In comparison, after reaction for 4 h, the –NCO signal at 2260 cm^{-1} decreased, confirming that $C_{16}H_{33}OH$ and IPDI were initially charged at equivalent molar quantities, and the reaction was considered to approach completeness at approx. 4 h.

3.2. Microencapsulation of C_{16}-IPDI. The OM recorded the typical formation process of microencapsulated C_{16}-IPDI as shown in Figure 4a–c. It could be seen that the MC was rather spherical (Figure 4b). At a higher magnification of SEM (Figure 4f–i), it was seen that the surface of the MCs was rough and it was covered with granular deposits. The generation of PUF nanoparticles was due to the precipitation in the aqueous solution of the prepolymer, and their aggregation on the surface of the capsule resulted in the roughness of the outer layer.

3.3. Sol–Gel Surface Treatment of C_{16}-IPDI MCs. To increase the efficiency of grafting and grafting density of the core material on the PUF shell, silane-functionalized MCs were prepared by co-condensation of TEOS with APTES (Scheme 2). This facile sol–gel surface treatment method is beneficial to generate a nanofilm to stabilize the surface roughness created by the agglomerated PUF particles.

In order to investigate the formation mechanism of the TEOS/APTES sol–gel layer on C_{16}-IPDI MCs, FTIR and XPS characterizations were carried out to explore the chemical composition on the surface of MCs. As shown in Figure 5, the absorption bands at 3029 and 2937 cm^{-1} were assigned to the asymmetric and symmetric stretching of C–H, respectively, and the peak at 874 cm^{-1} was observed due to the N–H bending vibration, suggesting the existence of amino groups in APTES-functionalized MCs. Furthermore, when the reaction was completed, the absorption bands at 1200 cm^{-1} corresponding to the C–O bonds disappeared, while the peak at 3385 cm^{-1} was significantly observed due to the –OH bending vibration, suggesting that TEOS/APTES hydrolysis and condensation occurred primarily at the chemical reaction phase and condensation took place at the later reaction phase between APTES and macroaggregated silica. In addition, the infrared spectrum of the sol–gel-treated specimens characteristically revealed extremely strong absorption peaks at 1144 and 1099 cm^{-1} corresponding to the asymmetric stretching vibration and the symmetric stretching vibration of Si–O–Si, respectively, indicating a condensation chemical reaction between Si–OH on silica and APTES to form a cross-linked structure on the MCs. Figure S1 (Supporting Information) shows the XPS spectra of untreated C_{16}-IPDI MCs and sol–gel-treated MCs, respectively. After the sol–gel surface treatment, fresh peaks at 150.6 and 102.2 eV due to Si 2s and Si 2p appeared in the spectrum of the sol–gel-treated MCs

https://dx.doi.org/10.1021/acsami.0c15455
ACS Appl. Mater. Interfaces 2020, 12, 57547–57559

Scheme 1. (a) Preparation of Superhydrophobic Sol−Gel-treated MCs; (b) Schematic Diagram Showing the Synthesis Route of Core Material (C_{16}-IPDI); (c) Schematic Illustration of the Procedure of Sol−Gel Surface Treatment Approach to Realize APTES-Functionalized MCs; (d) Schematic Description of the Hydrophilic to Superhydrophobic Transformation Process of Sol−Gel-treated MCs

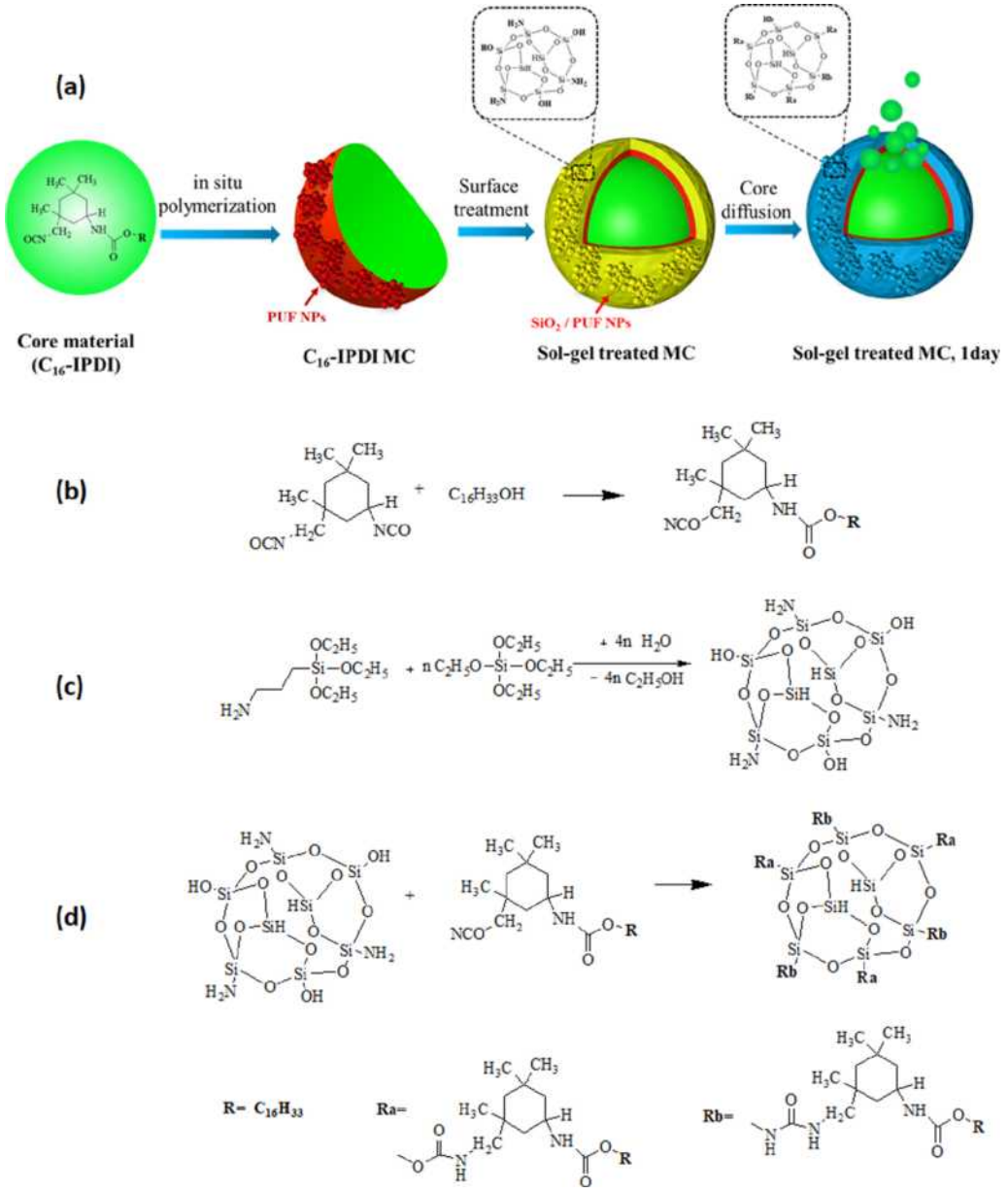

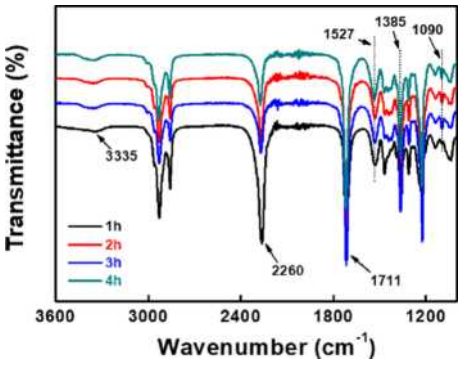

Figure 3. FTIR spectra of the hydrophobic core material (C_{16}-IPDI) at different reaction times.

(Table S1, Supporting Information). Furthermore, on comparison of the elemental weight percentage of untreated MCs, the weight percentages of sol−gel-treated MCs of Si, C, and O were 36.8, 39.6, and 22.8%, respectively, further indicating the successful formation of the TEOS/APTES surface on MCs.[46,47] Obviously, the XPS results were in agreement with the FTIR−ATR results.

3.4. Surface Morphology of Sol−Gel-treated MCs. Roughness also played an important role in the sol−gel-treated MC coating surface to achieve superhydrophobicity.[39] The SEM images revealed an obvious uniform "mountainlike" appearance on the PUF shell, and the NH_2−SiO_2 nanoparticles presented a mean size of 80 nm, generating cluster−cluster aggregation in the PUF layer, Figure S2 (Supporting Information). The topography profiles showing both three-

https://dx.doi.org/10.1021/acsami.0c15455
ACS Appl. Mater. Interfaces 2020, 12, 57547−57559

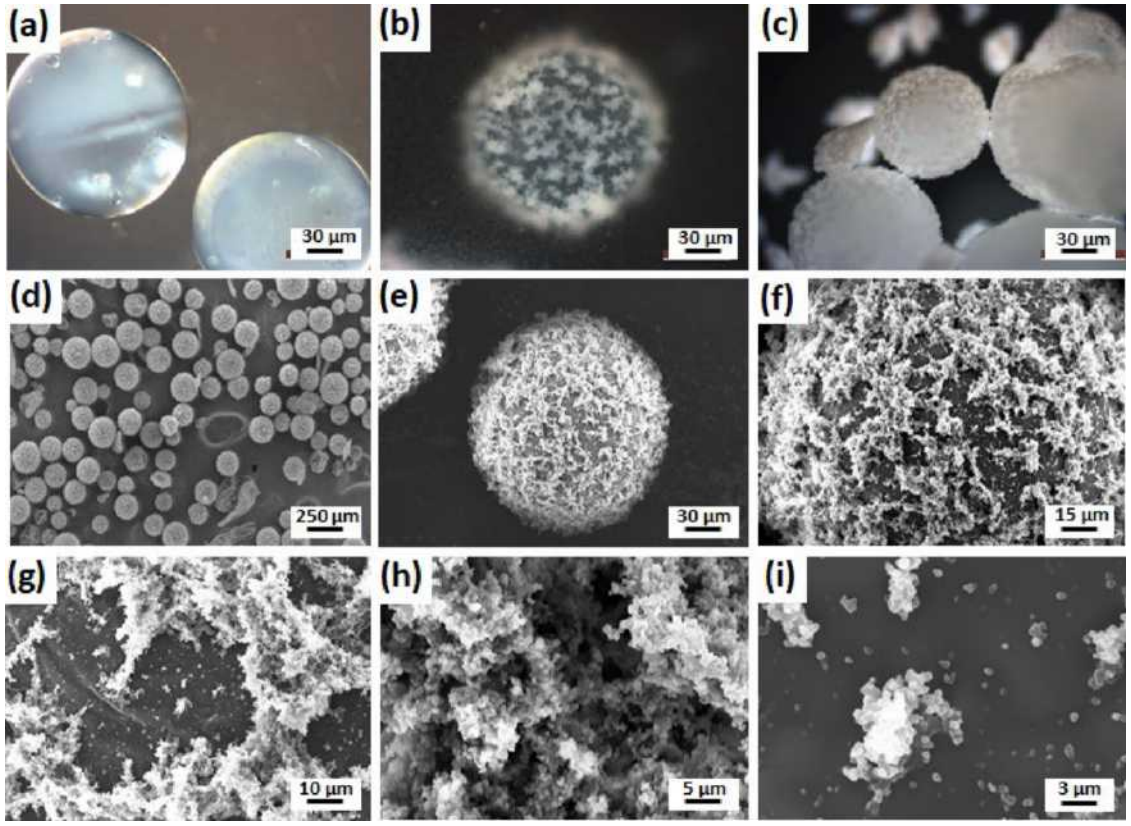

Figure 4. OM images of (a) oil droplets of C_{16}-IPDI suspension were obtained; (b) and (c) C_{16}-IPDI oil droplets were observed after emulsification for 15 min and 1 h, respectively; SEM morphology of the synthesized C_{16}-IPDI MCs: (d) overview of spherical-shaped C_{16}-IPDI MCs; (e) enlarged image of individual MC showing the rough outer surface; (f), (g), and (h) PUF nanoparticles deposited onto the surface of C_{16}-IPDI MCs; and (i) enlarged image of PUF nanoparticles on the shell wall.

Scheme 2. Schematic Illustration for Fabricating Superhydrophobic TEOS/APTES Hybrid Colloidal Particles with a Hierarchical Structure onto C_{16}-IPDI MCs using the Sol−Gel Surface Treatment Approach

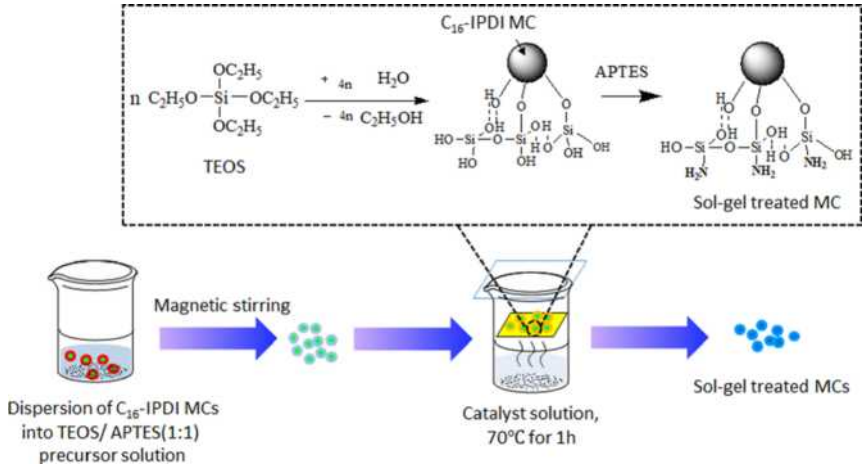

and two-dimensional images of pristine and modified MCs were shown in Figure S3 (Supporting Information). The surface of the untreated MC was rather rough, and the root-mean-square roughness was 3.81 nm due to the microstructure agglomerates of PUF resin particles. In contrast, the topography of the sol−gel-treated MC with a hierarchically structured surface was significantly transformed, and there was much relative cluster−cluster SiO_2 aggregation on the PUF shell, displaying a higher roughness value of 5.32 nm. This could be attributed to the fact that the APTES@silica layer was generated, and more SiO_2 particles were embedded on the Si−O−Si structure layer, roughing the nanoscale features. The other measurement for detecting surface roughness was by optical profilometry. It can characterize a larger area of the MC coating. Figure S4 (Supporting Information) showed that the surface roughness of the sol−gel-treated MC coating had a higher surface roughness than the untreated MC coating. This result was attributed to more SiO_2 particles embedded by the Si−O−Si structure layer, roughing the nanoscale features on the surface of MCs. In addition, the anodic voltage was

https://dx.doi.org/10.1021/acsami.0c15455
ACS Appl. Mater. Interfaces 2020, 12, 57547−57559

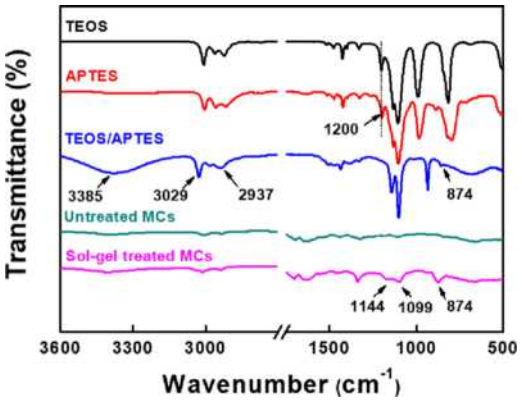

Figure 5. Comparison of FTIR spectra of TEOS, APTES, TEOS@APTES composite, C_{16}-IPDI MCs' shell, and sol−gel-treated MCs' shell.

increased on enhancing the surface roughness of the sol−gel-treated MC coating, and the heightened surface roughness was attributed to intensified sparks on the surface at a higher anodic voltage. Furthermore, the particle size of the sol−gel-treated MCs was about 150 μm, and the distribution was shown in Figure S5 (Supporting Information).

3.5. Wetting Properties of Sol−Gel-treated MCs. The sturdy sol−gel-treated MC coating that possessed superhydrophobic/superoleophilic properties was flexibly fabricated by embedding onto the surface of the cured epoxy matrix and applied on a galvanized sheet. The MC coating achieved superhydrophobicity with WCAs above 160° and superoleophilic effects (Figure 6). When the aging time was

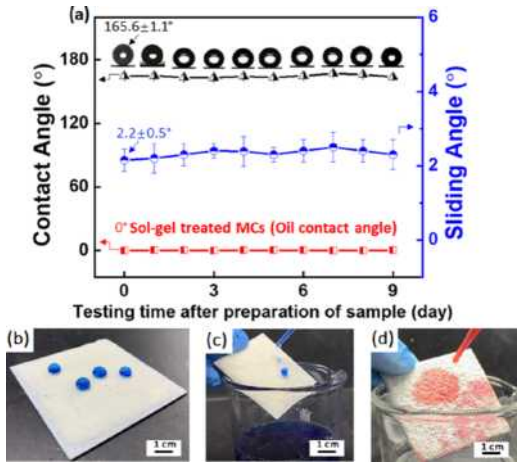

Figure 6. Surface properties of the sol−gel-treated MC coating: (a) water contact angles, sliding angles, and oil contact angles with the increasing time at room temperature; (b) still water droplets (dyed with blue color) on the coating and (c) a stream of water sliding off along with the coating; and (d) a stream of oil droplets (*n*-hexane dyed with Sudan III) spreading out and seeping into the coating.

increased, the WCAs of the sol−gel-treated MCs maintained a plateau of approximately 160°. This result was attributed to that the surface of MCs transferred from hydrophilic to superhydrophobic process with reaction time since the influence of the chemical reaction between the diffused core material (C_{16}-IPDI) and the NH_2−silica layer shell, which consumed the hydroxyl/amino groups by the isocyanate groups to generate a new low surface energy layer with enhanced superhydrophobicity on the surface of the sol−gel-treated MCs.

3.6. Durability and Solvent Resistance of Sol−Gel-treated MCs. In practical applications, oil−water separation materials must be sufficiently stable during the manufacturing processing cycle to withstand stringent conditions, such as UV, moisture, and solvent exposure.[48] In this work, in order to comprehensively assess the UV-resistant ability, the sol−gel-treated MC coatings were subjected to the UV aging test first. The results shown in Figure 7 showed that the changes in

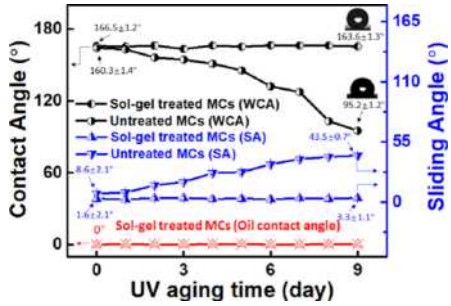

Figure 7. Surface properties of the sol−gel-treated MC coating under UV aging conditions: high-intensity wavelength UVA (340 nm) resistance of sol−gel untreated and treated MC coating, with observable influences on SAs and WCAs during 9 days of the UV aging test.

WCAs and SAs of the coatings after the UV aging test were significant. When the untreated MC coatings were kept in the weathering chamber for 9 days, their WCAs changed from 160.3 ± 1.4 to 95.2 ± 1.2° and the corresponding SAs changed from 8.6 ± 2.1 to 43.5 ± 0.7°. This trend can be explained by the possible decomposition of the rough PUF shells on some outermost MC surfaces. In addition, the WCAs of the sol−gel-treated MC coatings remained almost constant in the superhydrophobic state from 166.5 ± 1.2 to 163.6 ± 1.3° and the corresponding SAs showed a little change from 1.6 ± 2.1 to 3.3 ± 1.1° even after being exposed for 9 days in the same manner. Such excellent durability was possibly due to the thermal stability of C_{16}-SiO_2 and the security of the air-pocket layer stuck on the shell through TEOS@APTES covered on the surface of the macroaggregated PUF nanoparticles. Notably, the low SA values demonstrate that the sol−gel-treated MC coating still possesses superior water repellency despite the serious damage after the aging test. The outstanding resistance to weathering tests further demonstrated the formation of complete and compact C_{16}-SiO_2 superhydrophobic surfaces on the outer shells by the sol−gel vapor modification method.

Generally, synthesized PUF shells from organic polymers were prone to UV radiation degradation. The presence of UV-absorbing groups established sites where the polymer shell in the MC could undergo photo-oxidation leading to degradation. Furthermore, during UV absorption, on the conduction band, an electron jumped from the valence band, leaving a hole that was positively charged. These electrons and positively charged holes traveled to the surface of the MC shell, where they recombined or reacted with oxygen and water to form free radicals triggered by OH. These radicals also could be the factor accelerating the degradation of MCs.[31]

Sol−gel vapor surface treatment is an alternative method for improving the UV radiation resistance that was difficult to

https://dx.doi.org/10.1021/acsami.0c15455
ACS Appl. Mater. Interfaces 2020, 12, 57547−57559

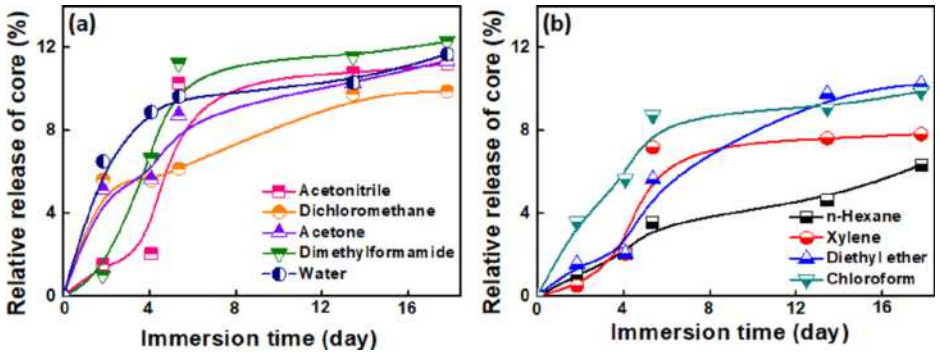

Figure 8. Relative released-out core material (C_{16}-IPDI) over testing times after submersion of MCs in polar aprotic solvents (e.g., DMF, acetonitrile, acetone, and DCM) and polar protic solvent (e.g., water) (a) and nonpolar organic solvents (e.g., *n*-hexane, diethyl ether, xylene, and chloroform) (b). In each solvent, the concentration of microcapsules was 16% by weight.

avoid degradation via traditional polymers. It was attributed to the chemical stabilization of the hydrolysis and condensation reactions from the sol−gel surface treatment for dense nanolayer formation, and this nanolayer covered the UV-absorbing groups on the original PUF shell so that UV light would not be absorbed. Furthermore, SiO_2 is an inorganic filler widely used in polymer composites since it has superior UV radiation resistance.[31−35] After the sol−gel vapor surface treatment process, the SiO_2 nanoparticles had been generated and incorporated into the nanolayer to inhibit the photocatalytic activity by disturbing the formation of radicals. The incorporation of SiO_2 nanoparticles has a possibility for improving the weathering performance of organic PUF microcapsules.[49]

Both the titration test and solvent immersion test were conducted to evaluate the long-term storage stability of sol−gel-treated MCs. Figure 8 illustrates that on increasing the immersion time in solvents, the released core material increased steadily. After submersion in various polar aprotic solvents for over 16 days, the final values were 11.2 wt % in acetonitrile, 11.4 wt % in acetone, 9.9 wt % in DCM, 11.3 wt % in DMF, and 11.3 wt % in polar protic water, as shown in Figure 8a. By contrast, the released core of the original core material was 6.3 wt % in *n*-hexane, 10.2 wt % in diethyl ether, 9.9 wt % in chloroform, and 7.8 wt % in xylene after the same testing time in various nonpolar organic solvents, as shown in Figure 8b. Basically, after being set in an organic solvent, thermosetting materials swell by imbibition.[50] The swelling ratio of a polymer had been reported to increase significantly with an increase in organic solvent polarity.[51] For instance, the sol−gel-treated MCs that were immersed in nonpolar organic solvents like xylene and *n*-hexane were hardly swollen and the PUF network of the shell remained unchanged, resulting in less release of core materials. When the polarity of aprotic solvent molecules was increased, the larger swelling ratio of MCs' shell led to the leakage of the liquid core upon chemical attacks. From Figure 8a, it is observed that the released-out core material increased significantly with solvent polarity. It could be because the higher polarity of the solvent was more likely to dissolve the SiO_2/PUF shell polar segments in compliance with the similar compatibility principle.[52] Therefore, the SiO_2/PUF shell as a polar material could lead to a weakened resistance to high polarity solvents due to the higher swelling ratio.[53]

Comparing the above titration test results with the previous test,[45] most titration values of the relative release percentage of core (C_{16}-IPDI) were below 12.0 wt % and achieved stabilization after over 16 days of the immersion test. Therefore, the sol−gel-treated MCs showed superior resistance to both polar aprotic solvents and nonpolar organic solvents. The leakage of C_{16}-IPDI loss in both nonpolar and polar aprotic solvents was mainly due to the fact that isocyanates were reactive with sol−gel-treated MCs' shell containing hydroxyl/amino groups. After swelling, the diffused isocyanates can undergo a reaction with hydroxyl/amino groups, producing new polyurethane aggregates distributed on the surface of the SiO_2/PUF MCs' shell. From the above investigation, this enormous enhancement in the solvent resistance was first due to the extremely cross-linked structure surface, which provided outstanding tightness that hindered the leakiness of the liquid core material once chemical attacks. In addition, the sol−gel-treated MCs exhibited outstanding superhydrophobicity (WCA > 160°) after over 20 days of solvent immersion test (Figure 9), verifying the outstanding solvent stability of the superhydrophobic surfaces.

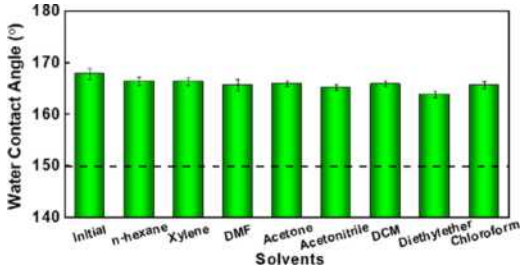

Figure 9. Superhydrophobicity of sol−gel-treated MCs after 20 days of immersion in various organic solvents.

3.7. Durable Oil−Water Separation Behaviors of Sol−Gel-treated MCs. In this work, the sol−gel-treated MCs with a hierarchical structure surface had been an ideal candidate for the highly effective filtration of oil contaminants from water, exhibiting superhydrophobicity and superoleophilicity. Figure 10a shows the mechanism of oil-in-water mixture separation by the sol−gel-treated MC coating. The oleophilic groups of the emulsifier existing in a continuous oil phase should be distributed in the surfactant-stabilized emulsions. Since the emulsifier was attached to the surface of the sol−gel-treated MCs, the emulsion came in contact with the surface of MCs, allowing the oil droplets to be absorbed. It was attributed to that the aggregates of these sol−gel-treated MCs had a hierarchical structure with a larger specific surface area

https://dx.doi.org/10.1021/acsami.0c15455
ACS Appl. Mater. Interfaces 2020, 12, 57547−57559

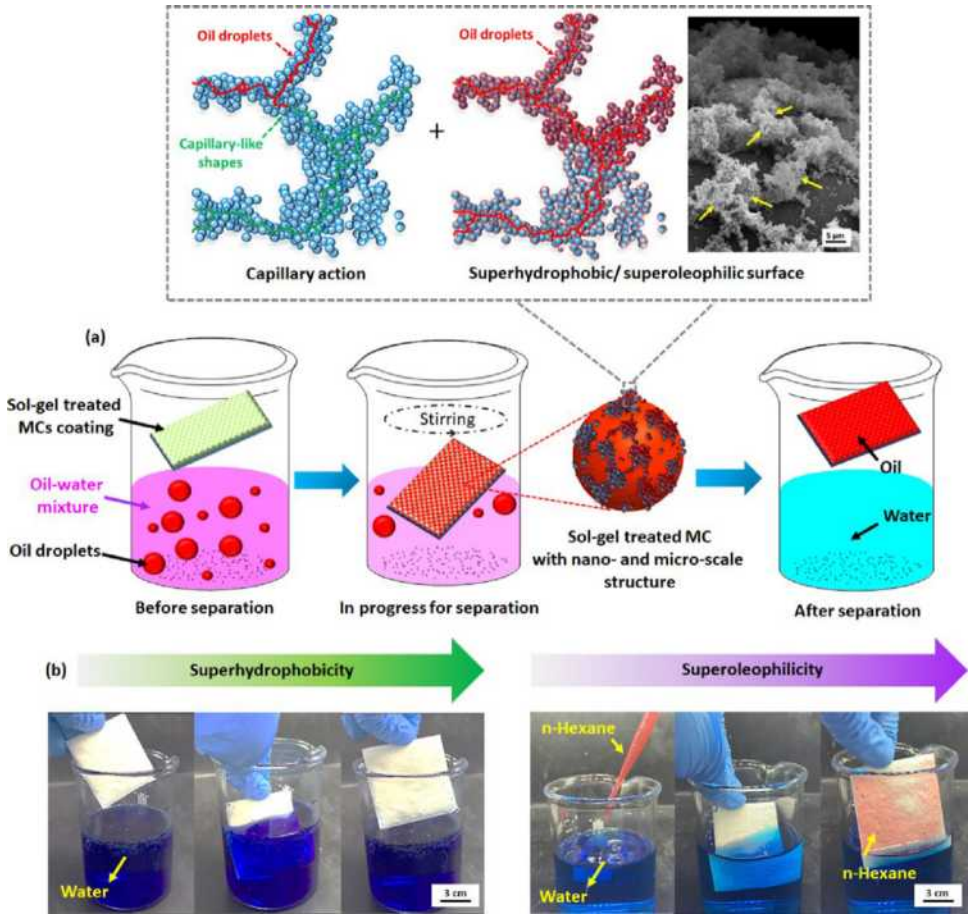

Figure 10. (a) Mechanism of oil-in-water separation performance by sol−gel-treated MC coating; demonstration of superhydrophobicity and superoleophilicity of sol−gel-treated MC-modified coatings: (b) blue color-dyed water and red color-dyed hexane in the blue color-dyed water mixture, respectively.

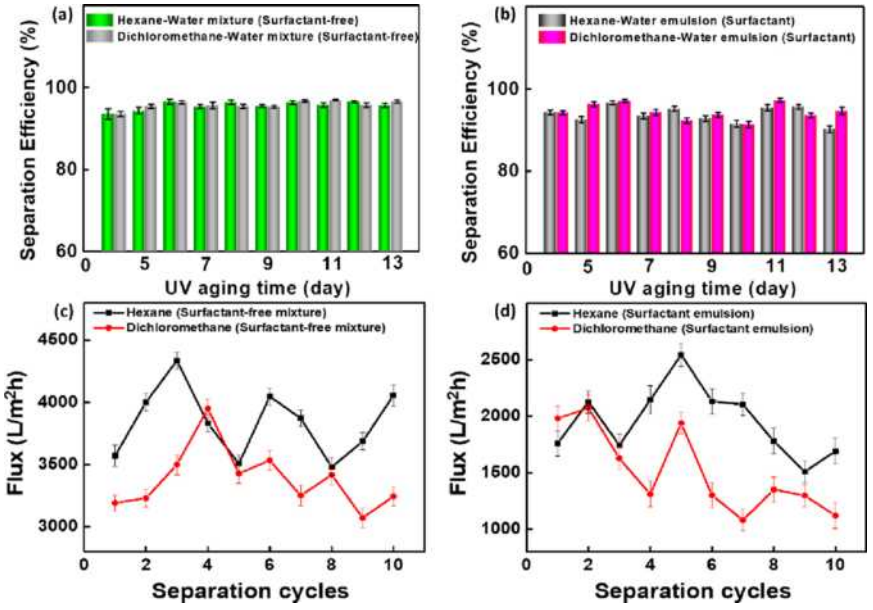

Figure 11. (a) Separation efficiency of surfactant-free oil−water mixture for 10 cycles after 13 days of UV aging treatment; (b) separation efficiency of surfactant-stabilized oil−water emulsion for 10 cycles after 13 days of UV aging treatment; (c) Infiltrate flux of oil−water mixture for separation by a T-junction filter with MCs; (d) Infiltrate flux of oil−water emulsion for separation by the vacuum-driven device with MCs.

compared with the sorbents or membranelike materials, providing more opportunities for superoleophilic surfaces to contact with the emulsion oil droplets.[39] In addition, the stacked pores of these hierarchical structure MCs have

https://dx.doi.org/10.1021/acsami.0c15455
ACS Appl. Mater. Interfaces 2020, 12, 57547−57559

Table 1. Information List of Various Methodologies and Materials Used for the Separation of Oil−Water Mixture or Emulsion

material	substrate	method	driver	flux (L/m^{2}h)	emulsion separation (Y or N)	reference
PDMS + TEOS	polyester textile	vapor−liquid sol−gel	gravity	N/A	N	39
POSS + PDMS	nylon membranes	dip-coated	syringe pump	200	Y	55
CNF−PDMS	stainless steel mesh	deposited	gravity	2970	Y	56
(PDVB)−PDMS	sponge and filtermembrane	in situ growth	vacuum pump	N/A	Y	57
PDMS	fibers	phase separation method	vacuum pump	2682	N	58
poly (ethylene glycol) diacrylate	membrane	phase inversion method	gravity	<100	N	59
polyvinylidene fluoride	membrane	coated	vacuum pump	700−3500	N	60
SiO_2−carbon	nanofibrous	electrospinning	gravity	>2000	N	61
APTES +TEOS	PUF microcapsule	sol−gel	vacuum pump	3000−4400	Y	This work

*N/A: not applicable

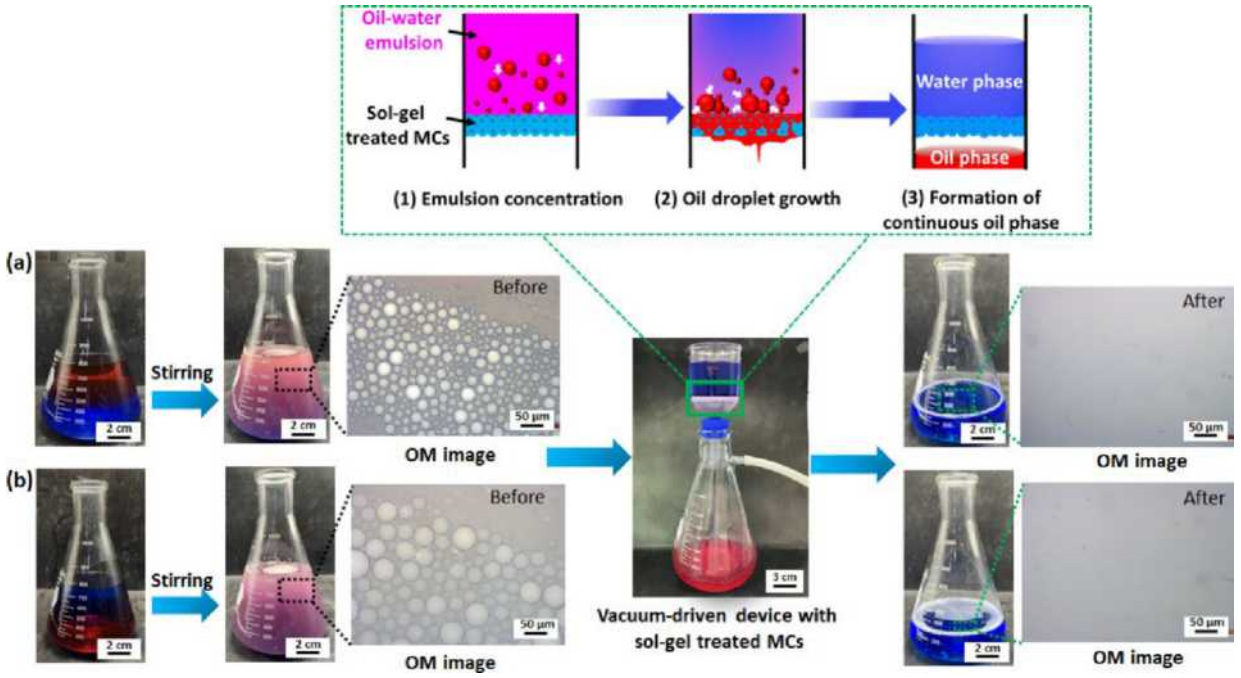

Figure 12. (a) Photograph of surfactant-stabilized oil (*n*-hexane dyed with Sudan III)/water (dyed with blue color) emulsion, water, and oil after separation by sol−gel-treated MCs from left to right; (b) photograph of surfactant-stabilized oil (DCM dyed with Sudan III)/water (dyed with blue color) emulsion, water, and oil after separation by sol−gel-treated MCs from left to right. (OM images showing the size of oil droplets in water). The vacuum-driven device consists of a nylon−(sol−gel-treated MC)−nylon sandwiched construction.

capillarylike shapes with nano- and microscale two-tier features, which had a beneficial effect on oil transfer and an adverse resistance to water transfer; therefore, the oil droplets could move through the stacked pores effectively, but the water did not.[54] As shown in Figure 10b, there were no blue color droplets left over the surface of the MC coating when it was pulled up from the dyed water. In addition, this superhydrophobic coating can selectively absorb *n*-hexane dyed with Sudan III on the water surface. Clearly, with the coating of the MCs immersed in a mixture of 3 mL of hexane and 200 mL of water, due to the superoleophilicity of the sol−gel-treated MCs, the oil easily penetrated the coating and water remained outside. The oil was finally completely extracted and almost 100% of the water was collected. Therefore, these robust MCs exhibited a high absorption rate for oil substances.

To separate a substantial quantity of an oil−water mixture or emulsion quickly by a labor-efficient industrial process, two kinds of oil−water separation devices were designed using the MCs as the filter material. A T-junction pipeline containing sol−gel-treated MCs was used to separate various oils like *n*-hexane and DCM from water (surfactant-free mixture) as demanded.

The separation efficiencies for hexane−water mixture and DCM−water mixture achieved were 95.6 and 95.7%, respectively, after using the filter apparatus (Figure 11a). Except for the separation efficiency, another parameter used in the separation assessment was the infiltrate flux; a higher infiltrate flux value in the filter device led to more fast separation. Herein, two kinds of filters were installed with superhydrophobic MCs, and the oil infiltrate fluxes of these filters were monitored for oil substances in mixture or emulsion. First, due to their different densities, heavy oil and light oil possibly presented distinct separation fluxes in mixtures by a T-junction filter, as shown in Figure 11c, and after the light oil was separated, the average infiltrate fluxes of hexane fluctuated from 3500 ± 89 to 4400 ± 68 L/m^2 h. After

https://dx.doi.org/10.1021/acsami.0c15455
ACS Appl. Mater. Interfaces 2020, 12, 57547−57559

the heavy oil was separated from the mixture, the average flux values of DCM in water were as low as 3100 ± 79 to 4000 ± 77 L/m^2 h. In addition, the effect of separation cycles on superhydrophobic MCs' separation efficiency, infiltrate flux, and UV aging time had been investigated as well. When the separation cycles increased to 10 times after 13 days of UV aging, the separation efficiency maintained above 90.0% for surfactant-free mixtures, and the average infiltrate fluxes of hexane and DCM in water were as high as 3839 ± 78 and 3473 ± 76 L/m^2 h, respectively, demonstrating extraordinary recyclability and reusability. The sol−gel-treated MCs displayed a substantial superiority in this study compared to the flux values of preliminary modified methodologies, as summarized in Table 1. It was attributed to the fact that the flux was closely related to the rough surfaces of the separation MCs, while the shell of MCs used in this work was favorably in capillarylike shapes with nano- and microscale two-tier features. The special shell of the MCs is compared with other oil−water separation materials (such as nylon textiles, PP fabrics, and PET films) reported in the preliminary papers, increasing more chance of superoleophilic surface area contact with the oil droplets. Therefore, without any external pressure, sol−gel-treated MCs can allow high flux separation. The scheme of the separation process of the hexane−water mixture by the pipeline apparatus is illustrated in Figure S6.

More interestingly, the sol−gel-treated MCs can also effectively separate surfactant-stabilized emulsions driven by a vacuum-driven device test. In order to recognize the progress of the effective oil droplet separation, sol−gel-treated MC-mediated oil droplet adsorption was investigated comprehensively. Before testing the separation behaviors, we observed the original hexane/DCM-in-water emulsion using a digital camera and an OM first. The results demonstrated that the emulsion consisted of numerous small oily bubbles, and the size distribution of emulsion droplet for two emulsions is 8−40 μm (Figure 12). After filtration using this system, it could be confirmed that the milky opaque droplets of oil−water emulsions became clear and transparent without any oil droplets after separation. The rate of separation of these two emulsions driven by the device showed almost no difference. Therefore, during the separation process, the superoleophilic shell surface of the sol−gel-treated MCs was able to capture these small oil droplets to amalgamate them. Finally, the separation efficiencies and reusability were subsequently investigated. Figure 11b,d shows that the separation efficiencies for hexane and DCM-in-water emulsion were 93.8 and 94.6%, respectively; the average infiltrate fluxes of hexane and DCM-in-water emulsion were as high as 2125 ± 67 and 1562 ± 69 L/m^2 h, respectively, after 10 cycles following 13 days of UV aging. On the whole, the distinct performance of the sol−gel-treated MCs shows the effectiveness and good reusable separation efficiency of surfactant-stabilized oil−water emulsion as well.

4. CONCLUSIONS

In summary, we reported a versatile strategy for fabricating sol−gel-treated MCs containing a hydrophobic core material (C_{16}-IPDI) with superior resistance to UV exposure and solvents. More importantly, it presented effective and reusable oil phase separation from water using these MCs through intrusion or gravity pressure trial designs. The main conclusions can be summarized as follows:

- The superhydrophobic/superoleophilic surface with a hierarchical structure was generated successfully on the MCs via highly versatile approaches of in situ polymerization and sol−gel surface treatment.
- The C_{16}-IPDI core material could diffuse spontaneously from the MCs mainly due to the fact that isocyanates were reactive with sol−gel-treated MCs' shell containing hydroxyl/amino groups. After the aging time was increased, the diffused isocyanates can undergo a reaction with hydroxyl/amino groups, producing new polyurethane aggregates distributed on the surface of SiO_2/PUF MCs' shell.
- The unique structure and superior tightness of MCs exhibited excellent resistance to 13 days of UV exposure as well as 20 days of immersion in polar and nonpolar organic solvents so that they showed outstanding UV-resistant and solvent-proof superhydrophobicity (WCAs >160°).
- Moreover, the MCs presented significant abilities to separate the surfactant-free and surfactant-stabilized oil phase from water effectively, achieving a high and reusable separation efficiency with over 90% oil purity and the high flux permitted the MCs to be applied in ultrafast and vacuum-driven oil−water separation after filtration even after 10 cycles with 13 days of UV aging treatment.

Therefore, the novel MCs have great potential applications in accidental oil spills and industrial wastewater treatments.

■ ASSOCIATED CONTENT

Supporting Information

The Supporting Information is available free of charge at https://pubs.acs.org/doi/10.1021/acsami.0c15455.

XPS spectra of untreated C_{16}-IPDI MCs and sol−gel-treated C_{16}-IPDI MCs; SEM images of the synthesized sol−gel-treated MCs: (a) overview of spherical-shaped sol−gel-treated MCs; (b) magnified image of single MC showing a rough outer shell; (c), (d), and (e) silica/PUF nanoparticles deposited onto the surface of sol−gel-treated MCs, and (f) magnified image of SiO_2 nanoparticles on the PUF shell; 3D surface constructions of AFM and corresponding 2D images of (a,b) C_{16}-IPDI MC surface and (c,d) sol−gel-treated MC surface. The scan area was 5 μm × 5 μm; surface roughness of untreated MC and treated MC coatings was investigated by optical profilometry with a scan area of 480 μm × 640 μm at different locations; particle size distribution of the sol−gel-treated MCs; scheme illustrating the separation process of the hexane−water mixture using the pipeline apparatus (PDF)

■ AUTHOR INFORMATION

Corresponding Authors

Yong Xiang − *School of Materials and Energy, University of Electronic Science and Technology of China, Chengdu 610064, China*; Email: xiang@uestc.edu.cn

Jinglei Yang − *Department of Mechanical and Aerospace Engineering, The Hong Kong University of Science and Technology, Hong Kong SAR, China*; orcid.org/0000-0002-9413-9016; Email: maeyang@ust.hk

https://dx.doi.org/10.1021/acsami.0c15455
ACS Appl. Mater. Interfaces 2020, 12, 57547−57559

Authors

Wenjun Luo − *Department of Mechanical and Aerospace Engineering, The Hong Kong University of Science and Technology, Hong Kong SAR, China*

Dawei Sun − *Department of Mechanical and Aerospace Engineering, The Hong Kong University of Science and Technology, Hong Kong SAR, China; College of Materials Science and Engineering, Beijing University of Technology, Beijing 100124, China*

Shusheng Chen − *Department of Mechanical and Aerospace Engineering, The Hong Kong University of Science and Technology, Hong Kong SAR, China*

Logesh Shanmugam − *Department of Mechanical and Aerospace Engineering, The Hong Kong University of Science and Technology, Hong Kong SAR, China*

Complete contact information is available at: https://pubs.acs.org/10.1021/acsami.0c15455

Notes

The authors declare no competing financial interest.

■ ACKNOWLEDGMENTS

The authors are grateful for the support from the Hong Kong University of Science and Technology (Grant #: R9365), the Guangzhou Municipal Science and Technology Bureau (Project #: 201907010024), the Technological Bureau of Guangzhou Huangpu District (Project #: 2018GH04), and the Zhongshan-HKUST Program (Project ID: RG066). The authors are also grateful to Ivan M L Sham and Sherry S P Bao from the Construction and Building department of Nano and Advanced Materials Institute Limited (NAMI) for their generous help.

■ REFERENCES

(1) Al-Majed, A. A.; Adebayo, A. R.; Hossain, M. E. A Sustainable Approach to Controlling Oil Spills. *J. Environ. Manage.* **2012**, *113*, 213−227.

(2) Raturi, P.; Yadav, K.; Singh, J. P. ZnO-Nanowires-Coated Smart Surface Mesh with Reversible Wettability for Efficient On-Demand Oil/Water Separation. *ACS Appl. Mater. Interfaces* **2017**, *9*, 6007−6013.

(3) Wang, J.; Wang, H.; Geng, G. Flame-Retardant Superhydrophobic Coating Derived from Fly Ash on Polymeric Foam for Efficient Oil/Corrosive Water and Emulsion Separation. *J. Colloid Interface Sci.* **2018**, *525*, 11−20.

(4) Kintisch, E. An Audacious Decision in Crisis Gets Cautious Praise. *Science* **2010**, *329*, 735.

(5) Li, A.; Sun, H.-X.; Tan, D.-Z.; Fan, W.-J.; Wen, S.-H.; Qing, X.-J.; Li, G.-X.; Li, S.-Y.; Deng, W.-Q. Superhydrophobic Conjugated Microporous Polymers for Separation and Adsorption. *Energy Environ. Sci.* **2011**, *4*, 2062−2065.

(6) Shannon, M. A.; Bohn, P. W.; Elimelech, M.; Georgiadis, J. G.; Mariñas, B. J.; Mayes, A. M. Science and Technology for Water Purification in the Coming Decades. *Nature* **2008**, *452*, 301−310.

(7) Wang, C.; Yao, T.; Wu, J.; Ma, C.; Fan, Z.; Wang, Z.; Cheng, Y.; Lin, Q.; Yang, B. Facile Approach in Fabricating Superhydrophobic and Superoleophilic Surface for Water and Oil Mixture Separation. *ACS Appl. Mater. Interfaces* **2009**, *1*, 2613−2617.

(8) Kong, Z.; Wang, J.; Lu, X.; Zhu, Y.; Jiang, L. In situ Fastening Graphene Sheets into a Polyurethane Sponge for the Highly Efficient Continuous Cleanup of Oil spills. *Nano Res.* **2017**, *10*, 1756−1766.

(9) Wang, B.; Liang, W.; Guo, Z.; Liu, W. Biomimetic Super-Lyophobic and Super-Lyophilic Materials Applied for Oil/Water Separation: a New Strategy Beyond Nature. *Chem. Soc. Rev.* **2015**, *44*, 336−361.

(10) Wang, J.; Shi, Z.; Fan, J.; Ge, Y.; Yin, J.; Hu, G. Self-Assembly of Graphene into Three-Dimensional Structures Promoted by Natural Phenolic Acids. *J. Mater. Chem.* **2012**, *22*, 22459−22466.

(11) Howarter, J. A.; Youngblood, J. P. Amphiphile Grafted Membranes for the Separation of Oil-in-Water Dispersions. *J. Colloid Interface Sci.* **2009**, *329*, 127−132.

(12) Tian, D.; Zhang, X.; Tian, Y.; Wu, Y.; Wang, X.; Zhai, J.; Jiang, L. Photo-Induced Water-Oil Separation Based on Switchable Superhydrophobicity-Superhydrophilicity and Underwater Superoleophobicity of the Aligned ZnO Nanorod Array-Coated Mesh Films. *J. Mater. Chem.* **2012**, *22*, 19652−19657.

(13) Chen, L.; Du, R.; Zhang, J.; Yi, T. Density Controlled Oil Uptake and Beyond: From Carbon Nanotubes to Graphene Nanoribbon Aerogels. *J. Mater. Chem. A* **2015**, *3*, 20547−20553.

(14) Sun, H.; Xu, Z.; Gao, C. Multifunctional, Ultra-Flyweight, Synergistically Assembled Carbon Aerogels. *Adv. Mater.* **2013**, *25*, 2554−2560.

(15) Wu, Z.-Y.; Li, C.; Liang, H.-W.; Zhang, Y.-N.; Wang, X.; Chen, J.-F.; Yu, S.-H. Carbon Nanofiber Aerogels for Emergent Cleanup of Oil Spillage and Chemical Leakage under Harsh Conditions. *Sci. Rep.* **2015**, *4*, 4079.

(16) Si, Y.; Fu, Q.; Wang, X.; Zhu, J.; Yu, J.; Sun, G.; Ding, B. Superelastic and Superhydrophobic Nanofiber-Assembled Cellular Aerogels for Effective Separation of Oil/Water Emulsions. *ACS Nano* **2015**, *9*, 3791−3799.

(17) Xu, L.; Xiao, G.; Chen, C.; Li, R.; Mai, Y.; Sun, G.; Yan, D. Superhydrophobic and Superoleophilic Graphene Aerogel Prepared by Facile Chemical Reduction. *J. Mater. Chem. A* **2015**, *3*, 7498−7504.

(18) Zhao, Y.; Hu, C.; Hu, Y.; Cheng, H.; Shi, G.; Qu, L. A Versatile, Ultralight, Nitrogen-Doped Graphene Framework. *Angew. Chem. Int. Ed.*. **2012**, *51*, 11371−11375.

(19) Gui, X.; Zeng, Z.; Lin, Z.; Gan, Q.; Xiang, R.; Zhu, Y.; Cao, A.; Tang, Z. Magnetic and Highly Recyclable Macroporous Carbon Nanotubes for Spilled Oil Sorption and Separation. *ACS Appl. Mater. Interfaces* **2013**, *5*, 5845−5850.

(20) Chen, N.; Pan, Q. Versatile Fabrication of Ultralight Magnetic Foams and Application for Oil-Water Separation. *ACS Nano* **2013**, *7*, 6875−6883.

(21) Zhu, L.; Chen, M.; Dong, Y.; Tang, C. Y.; Huang, A.; Li, L. A Low-Cost Mullite-Titania Composite Ceramic Hollow Fiber Microfiltration Membrane for Highly Efficient Separation of Oil-in-Water Emulsion. *Water Res.* **2016**, *90*, 277−285.

(22) Zhang, X.; Shi, F.; Niu, J.; Jiang, Y.; Wang, Z. Superhydrophobic Surfaces: From Structural Control to Functional Application. *J. Mater. Chem.* **2008**, *18*, 621−633.

(23) Zhu, Y.; Wang, D.; Jiang, L.; Jin, J. Recent Progress in Developing Advanced Membranes for Emulsified Oil/Water Separation. *NPG Asia Mater.* **2014**, *6*, e101−e101.

(24) Yu, L.; Han, M.; He, F. A Review of Treating Oily Wastewater. *Arab. J. Chem.* **2017**, *10*, S1913−S1922.

(25) Liu, Y.; Zhu, W.; Guan, K.; Peng, C.; Wu, J. Preparation of High Permeable Alumina Ceramic Membrane with Good Separation Performance via UV curing technique. *RSC Adv.* **2018**, *8*, 13567−13577.

(26) Gutberlet, J. Informal and Cooperative Recycling as a Poverty Eradication Strategy. *Geo. Comp.* **2012**, *6*, 19−34.

(27) Bhushan, B. Biomimetics Inspired Surfaces for Drag Reduction and Oleophobicity/Philicity. *Beilstein J. Nanotechnol.* **2011**, *2*, 66−84.

(28) Lafuma, A.; Quéré, D. Superhydrophobic States. *Nat. Mater.* **2003**, *2*, 457−460.

(29) Yao, X.; Song, Y.; Jiang, L. Applications of Bio-Inspired Special Wettable Surfaces. *Adv. Mater.* **2011**, *23*, 719−734.

(30) Cassie, A. B. D.; Baxter, S. Wettability of Porous Surfaces. *Trans. Faraday Soc.* **1944**, *40*, 546−551.

(31) Zhu, Q.; Pan, Q.; Liu, F. Facile Removal and Collection of Oils from Water Surfaces through Superhydrophobic and Superoleophilic Sponges. *J. Phys. Chem. C* **2011**, *115*, 17464−17470.

(32) Zhang, H.; Li, Y.; Xu, Y.; Lu, Z.; Chen, L.; Huang, L.; Fan, M. Versatile Fabrication of a Superhydrophobic and Ultralight Cellulose-

Based Aerogel for Oil Spillage Clean-up. *Phys. Chem. Chem. Phys.* **2016**, *18*, 28297−28306.
(33) Ke, Q.; Jin, Y.; Jiang, P.; Yu, J. Oil/Water Separation Performances of Superhydrophobic and Superoleophilic Sponges. *Langmuir* **2014**, *30*, 13137−13142.
(34) Li, Z.-T.; He, F.-A.; Lin, B. Preparation of Magnetic Superhydrophobic Melamine Sponge for Oil-Water Separation. *Powder Technol.* **2019**, *345*, 571−579.
(35) Su, B.; Tian, Y.; Jiang, L. Bioinspired Interfaces with Superwettability: From Materials to Chemistry. *J. Am. Chem. Soc.* **2016**, *138*, 1727−1748.
(36) Xiao, C.; Si, L.; Liu, Y.; Guan, G.; Wu, D.; Wang, Z.; Hao, X. Ultrastable Coaxial Cable-Like Superhydrophobic Mesh with Self-Adaption Effect: Facile Synthesis and Oil/Water Separation Application. *J. Mater. Chem. A* **2016**, *4*, 8080−8090.
(37) Shi, Z.; Zhang, W.; Zhang, F.; Liu, X.; Wang, D.; Jin, J.; Jiang, L. Ultrafast Separation of Emulsified Oil/Water Mixtures by Ultrathin Free-Standing Single-Walled Carbon Nanotube Network Films. *Adv. Mater.* **2013**, *25*, 2422−2427.
(38) Yu, L.; Zhang, S.; Zhang, M.; Chen, J. Superhydrophobicity Construction with Dye-Sensitised TiO_2 on Fabric Surface for Both Oil/Water Separation and Water Bulk Contaminants Purification. *Appl. Surf. Sci.* **2017**, *425*, 46−55.
(39) Su, X.; Li, H.; Lai, X.; Zhang, L.; Wang, J.; Liao, X.; Zeng, X. Vapor-Liquid Sol-Gel Approach to Fabricating Highly Durable and Robust Superhydrophobic Polydimethylsiloxane@Silica Surface on Polyester Textile for Oil-Water Separation. *ACS Appl. Mater. Interfaces* **2017**, *9*, 28089−28099.
(40) Xue, C.-H.; Guo, X.-J.; Zhang, M.-M.; Ma, J.-Z.; Jia, S.-T. Fabrication of Robust Superhydrophobic Surfaces by Modification of Chemically Roughened Fibers via Thiol-ene Click Chemistry. *J. Mater. Chem. A* **2015**, *3*, 21797−21804.
(41) Barthlott, W.; Mail, M.; Neinhuis, C. Superhydrophobic Hierarchically Structured Surfaces in Biology: Evolution, Structural Principles and Biomimetic Applications. *Philos. Trans. A Math. Phys. Eng. Sci.* **2016**, *374*, 20160191.
(42) Ge, M.; Cao, C.; Huang, J.; Zhang, X.; Tang, Y.; Zhou, X.; Zhang, K.; Chen, Z.; Lai, Y. Rational Design of Materials Interface at Nanoscale Towards Intelligent Oil-Water Separation. *Nano. Horizons* **2018**, *3*, 235−260.
(43) Han, X.; Hu, J.; Chen, K.; Wang, P.; Zhang, G.; Gu, J.; Ding, C.; Zheng, X.; Cao, F. Self-Assembly and Epitaxial Growth of Multifunctional Micro-Nano-Spheres for Effective Separation of Water-in-Oil Emulsions with Ultra-High Flux. *Chem. Eng. J.* **2018**, *352*, 530−538.
(44) Brown, E. N.; Kessler, M. R.; Sottos, N. R.; White, S. R. In situ Poly(urea-formaldehyde) Microencapsulation of Dicyclopentadiene. *J. Microencapsulation* **2010**, *20*, 719−730.
(45) Wu, G.; An, J.; Tang, X.-Z.; Xiang, Y.; Yang, J. A Versatile Approach towards Multifunctional Robust Microcapsules with Tunable, Restorable, and Solvent-Proof Superhydrophobicity for Self-Healing and Self-Cleaning Coatings. *Adv. Funct. Mater.* **2014**, *24*, 6751−6761.
(46) Zhang, X.; Chen, L.; Yun, J.; Wang, X.; Kong, J. Constructing Magnetic Si-C-Fe Hybrid Microspheres for Room Temperature Nitroarenes reduction. *J. Mater. Chem. A* **2017**, *5*, 10986−10997.
(47) Xu, W.; Rhee, S.-W. Low-Operating Voltage Organic Field-Effect Transistors with High-k Cross-Linked Cyanoethylated Pullulan Polymer Gate Dielectrics. *J. Mater. Chem.* **2009**, *19*, 5250−5257.
(48) Li, B.; Zhang, J. Durable and Self-Healing Superamphiphobic Coatings Repellent Even to Hot Liquids. *Chem. Commun.* **2016**, *52*, 2744−2747.
(49) Xiong, M.; Ren, Z.; Liu, W. Fabrication of Superhydrophobic and UV-Resistant Surface on Cotton Fabric via Layer-By-Layer Assembly of Silica-Based UV Absorber. *J. Dispersion Sci. Technol.* **2020**, *41*, 1703−1710.
(50) Flory, P. J.; Rehner, J. Statistical Mechanics of Cross-Linked Polymer Networks II Swelling. *J. Chem. Phys.* **1943**, *11*, 521−526.
(51) Sun, D.; An, J.; Wu, G.; Yang, J. Double-Layered Reactive Microcapsules with Excellent Thermal and Non-Polar Solvent Resistance for Self-Healing Coatings. *J. Mater. Chem. A* **2015**, *3*, 4435−4444.
(52) Schneider, N. S.; Illinger, J. L.; Cleaves, M. A. Liquid Sorption in a Segmented Polyurethane Elastomer. *Polym. Eng. Sci.* **1986**, *26*, 1547−1551.
(53) Jonquières, A.; Roizard, D.; Lochon, P. Use of Empirical Polarity Parameters to Describe Polymer/Liquid Interactions: Correlation of Polymer Swelling with Solvent Polarity in Binary and Ternary Systems. *J. Appl. Polym. Sci.* **1994**, *54*, 1673−1684.
(54) Song, Y.; Zhou, J.; Fan, J.-B.; Zhai, W.; Meng, J.; Wang, S. Hydrophilic/Oleophilic Magnetic Janus Particles for the Rapid and Efficient Oil-Water Separation. *Adv. Funct. Mater.* **2018**, *28*, 1802493.
(55) Kwon, G.; Kota, A. K.; Li, Y.; Sohani, A.; Mabry, J. M.; Tuteja, A. On-Demand Separation of Oil-Water Mixtures. *Adv. Mater.* **2012**, *24*, 3666−3671.
(56) Lin, X.; Heo, J.; Jeong, H.; Choi, M.; Chang, M.; Hong, J. Robust Superhydrophobic Carbon Nanofiber Network Inlay-Gated Mesh for Water-in-Oil Emulsion Separation with High flux. *J. Mater. Chem. A* **2016**, *4*, 17970−17980.
(57) Li, Y.; Zhang, Z.; Wang, M.; Men, X.; Xue, Q. One-Pot Fabrication of Nanoporous Polymer Decorated Materials: from Oil-Collecting Devices to High-Efficiency Emulsion Separation. *J. Mater. Chem. A* **2017**, *5*, 5077−5087.
(58) Xue, C.-H.; Li, Y.-R.; Hou, J.-L.; Zhang, L.; Ma, J.-Z.; Jia, S.-T. Self-Roughened Superhydrophobic Coatings for Continuous Oil-Water Separation. *J. Mater. Chem. A* **2015**, *3*, 10248−10253.
(59) Chakrabarty, B.; Ghoshal, A. K.; Purkait, M. K. Ultrafiltration of Stable Oil-in-Water Emulsion by Polysulfone Membrane. *J. Membr. Sci.* **2008**, *325*, 427−437.
(60) Klionsky, D. J. Guidelines for The Use and Interpretation of Assays for Monitoring Autophagy (3rd edition). *Autophagy* **2016**, *12*, 1−222.
(61) Tai, M. H.; Gao, P.; Tan, B. Y. L.; Sun, D. D.; Leckie, J. O. Highly Efficient and Flexible Electrospun Carbon-Silica Nanofibrous Membrane for Ultrafast Gravity-Driven Oil-Water Separation. *ACS Appl. Mater. Interfaces* **2014**, *6*, 9393−9401.

https://dx.doi.org/10.1021/acsami.0c15455
ACS Appl. Mater. Interfaces 2020, 12, 57547−57559